Numerical and Experimental Investigation of Tandem Wing Flyers

Thomas Lambert*
University of Liège, 4000 Liège, Belgium

Nicolas Warbecq† and Patrick Hendrick‡
Université Libre de Bruxelles, 1050 Bruxelles, Belgium

Robert Nudds§
Manchester University, Manchester, UK

Thomas Andrianne¶ and Grigorios Dimitriadis‖
University of Liège, 4000 Liège, Belgium

The recent focus on micro-UAV systems and bio-inspired drones has generated interest in tandem wing applications. Dragonfly-based configurations are of significance for very low Reynolds numbers; for larger drones, Microraptor-based geometries could prove to be efficient. The present study of tandem wing flyers aims at understanding the basic principles governing the aerodynamic properties of tandem wings in close proximity. The analysis includes both numerical simulations by means of the Unsteady Vortex Lattice Method and wind tunnel experimentation applied to generic rectangular wing geometries. Preliminary conclusions include the facts that increasing the rear wing's angle of attack results in a bigger increase in lift than increasing the front wing's angle of attack. The dihedral angles of the two wings also seem to have significant impact on the lift, some configurations leading to an increase in lift coefficient of up to 25%. The insight provided by the results will be used in the future to test and validate different flight configurations for the *Microraptor* and, hopefully, to shed some light on its preferred in-flight configuration and its flight capabilities.

I. Introduction

The denomination "tandem wings" encompasses many sub-configurations such as "true tandem", Delanne wings, canard, closed wings and biplanes. Most of these have been studied since the very early age of manned flight. During the second world war, researchers attempted to describe as accurately as possible the advantages and disadvantages of such systems [1]. However, most of the research effort was eventually directed towards advances in single-wing configurations, so that tandem wing geometries lagged behind in development. Nowadays, only the canard configuration is common, especially for jet fighters; other tandem wing configurations concern either sensorcraft applications (see for example Fig. 1(a)) or are purely experimental (Fig. 1(b)).

The recent focus on micro-UAV systems and bio-inspired drones has generated renewed enthusiasm in tandem wing applications[2, 3]. For example, configurations based on the dragonfly (such as DSTL's Skeeter) are of interest for very small Reynolds number applications. Besides the dragonfly, it is believed that several other species of biological tandem wing flyers have existed. Some flying dinosaur specimens were discovered in recent years that featured large feathered hind limbs. The most notable example is probably the *Microraptor Gui* discovered in China in 2001 [4]. Since its discovery, several biologists have tried to reconstruct its general shape and determine how it was able to fly or

*Ph.D. Student, Aerospace and Mechanical Engineering Department, University of Liège, Quartier Polytech, Allée de la découverte, 9, 4000 Liège, Belgium, AIAA Student Member. t.lambert@uliege.be

†Master Student, Aero-Thermo-Mechanics, Université Libre de Bruxelles, Avenue F.D. Roosevelt 50 CP 165/41, 1050 Brussels, Belgium.

‡Professor, Aero-Thermo-Mechanics, Université Libre de Bruxelles, Avenue F.D. Roosevelt 50 CP 165/41, 1050 Brussels, Belgium.

§Professor, Division of Evolution & Genomic Sciences, Manchester University, Manchester M13 9PT, UK.

¶Permanent Researcher, Aerospace and Mechanical Engineering Department, University of Liège, Quartier Polytech, Allée de la découverte, 9, 4000 Liège, Belgium, AIAA Member.

‖Associate Professor, Aerospace and Mechanical Engineering Department, University of Liège, Quartier Polytech, Allée de la découverte, 9, 4000 Liège, Belgium, AIAA Senior Member.

(a) Xianglong UAV [pinterest.co.uk]

(b) Proteus, Scaled Composites [wikipedia.org]

Fig. 1 Examples of current and future tandem wing aircraft projects.

glide. Researchers are still uncertain about the flying capabilities of the specimen and no clear consensus seems to have been achieved yet [5–7]. This specimen is very important for the understanding of the evolution of avian flight, as *Microraptor* seems to be the oldest vertebrate capable of flying. Currently the flight posture of the *Microraptor* is still a hot topic among biologists.

The present study of tandem wing flyers aims at understanding the basic principles governing the aerodynamic properties of tandem wings in close proximity during steady flight. The analysis includes both numerical simulations by means of the Unsteady Vortex Lattice Method and wind tunnel experimentation applied to generic rectangular wing geometries. The insight provided by the results will be used in the future to test and validate different flight configurations for the *Microraptor* and, hopefully, to shed some light on its preferred in-flight configuration and its flight capabilities.

Fig. 2 Holotype specimen of the Microraptor [Institute of Vertebrate Paleontology and Paleoanthropology (IVPP) V13352] [6] – Proposed representation of the Microraptor. Scale bar, 6 cm [4].

II. Wind Tunnel Model

A. Model design

In order to keep the study as general as possible, the wings were chosen to be rectangular, un-cambered and identical. A NACA 0012 profile was selected for convenience and ease of manufacturing. The span of each individual wing was set to $b = 20$ cm, and the chord to $c = 6.25$ cm, leading to an aspect ratio of $AR = 6.4$. The wings were printed in polyamide using the laser sintering method of 3D additive manufacturing. In order to reinforce the wings' structure and

limit their deflection, an aluminum rod was inserted at the maximum thickness point of the wing (30% of the chord, measured from the leading edge). This rod was also used to clamp each wing to the main structure. The clamping mechanism was designed to allow for many different configurations and to maintain the wings in the appropriate position during the tests. Simple clamping devices usually employed for dial indicators were chosen, as they allow to control the dihedral and pitch angles and the vertical position of the wings with the use of a single bolt.

For convenience, four rods were placed on the support plate, one for each half-wing. The rods corresponding to the front wings were fixed to the support, while the ones for the aft wings could be bolted in different places, allowing for the variation in the horizontal distance between the front and aft wings. A fairing was also designed and placed around the clamping mechanism, in order to reduce as much as possible the perturbation of the flow by the support and clamping mechanism. This part was essentially a fuselage or body and it was also 3D printed using the same technique as for the wings. The main geometrical parameters of the model are summed up in Table 1.

Parameter	**Symbol**	**Value**	**Unit**
Wing Chord	c	0.0625	[m]
Wing Span	b	0.2	[m]
Wing Profile	-	NACA 0012	
Body Chord	c_b	0.256	[m]
Body Span	b_b	0.1	[m]

Table 1 Main geometrical parameters of the model.

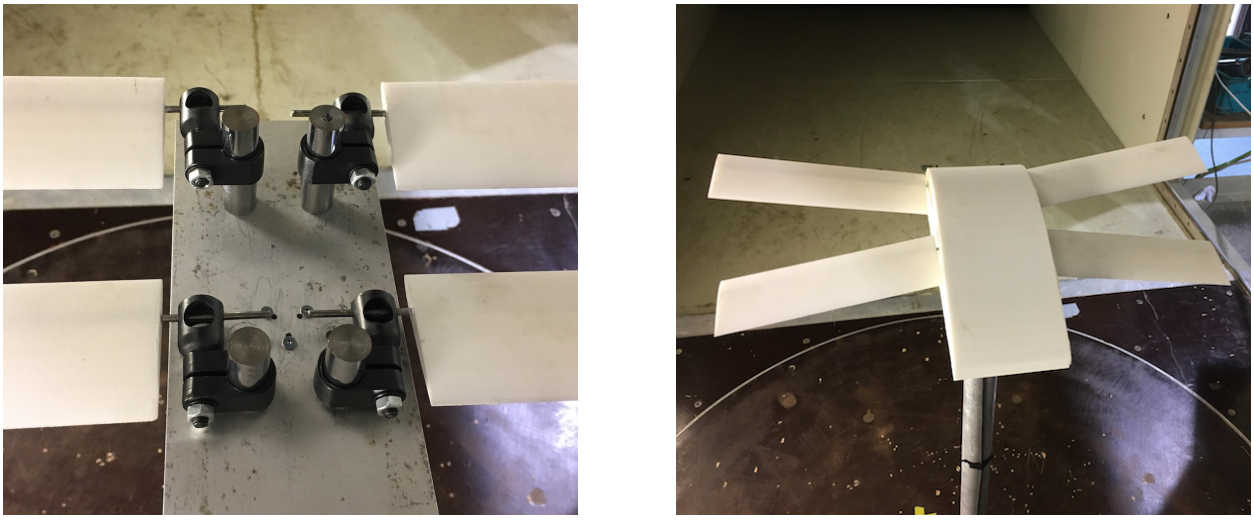

Fig. 3 Clamping mechanism (left). – Model in wind tunnel (right).

B. Wind tunnel testing

The wind tunnel tests were carried out in the large subsonic wind tunnel of the University of Liège. The aerodynamic forces and moments acting on the model were measured by means of an ATI 6-component load sensor, attached to the bottom plate of the clamping mechanism. Consequently, the total lift and drag of the entire body and wing assembly were measured using this sensor.

A first set of tests was conducted on the model without the wings, in order to quantify the impact of the mount, support and fairing on the measurements. Those measurements were later used to calibrate the body's numerical model

by ensuring it generates as much lift as the experimental fuselage.

III. Numerical model

The numerical simulations were carried out using the Unsteady Vortex Lattice Method (UVLM), as described by Katz and Plotkin [8]. This lifting surface method assumes potential incompressible flow and is well suited to study the interactions between multiple bodies. An in-house UVLM code [9, 10] was adapted to tandem wing geometries. In order to match as accurately as possible the wind tunnel experiments, the four wings and the body were included in the numerical model. The wings' dimensions and profile were set to match exactly the physical model used in the wind tunnel (see Table 1). Following the assumption of the vortex lattice approach, the thickness of the wings is ignored, so that the latter are represented as uncambered rectangular flat plates. The numerical representation of the body matches the chord and span of the experimental one. However, its camber line was adjusted so that the lift computed numerically fits the one measured in the wind tunnel on the isolated body. Furthermore, as the UVLM does not calculate viscous drag, the latter was inferred from the difference between the induced drag calculated by the UVLM and the total drag measured from the experiments. The body's viscous drag was simply added to all numerical results to better compare the outcomes of the simulations to the total forces measured in the wind tunnel.

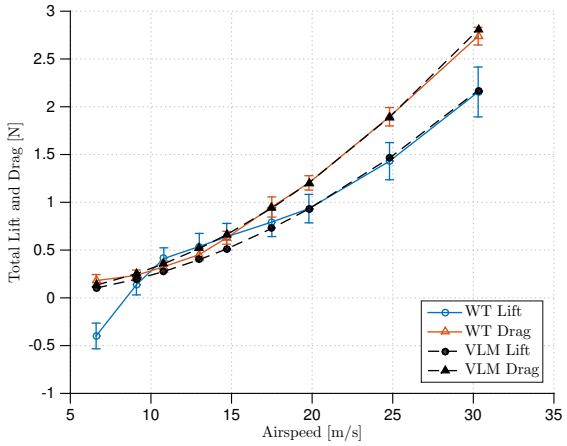

Fig. 4 Comparison of the numerical and experimental body (and mount) loads.

A comparison of the aerodynamic loads for the experimental and numerical body is shown in Fig. 4. The VLM body was calibrated to match exactly the wind tunnel measurements carried out at 20 m/s, so that the numerical and experimental data are identical at this airspeed. Nevertheless, good agreement between the two sets of results is obtained for all airspeeds between 18 and 30 m/s.

The UVLM mesh for each element (body and wings) is composed of 18 spanwise and 12 chordwise panels. For the wings, the individual panels have all the same chord but their span is defined using a half-cosine rule in order to obtain smaller panels at the tips and, hence, better capture 3D flow effects. For the body, a half-cosine spacing rule is used in the spanwise direction and a cosine rule is employed for the chordwise direction so that panels are smaller at the leading edge than at the trailing edge.

A free-wake model was employed to better capture the mutual interaction of the different wakes. Due to the strong interactions between the wakes of the four wings and body, the calculations of the induced velocities in the wakes were carried out by means of the Vatistas model [11] instead of the typical Biot-Savart law used in [8]. The Biot-Savart law is usually not a good choice when it comes to representing wakes that lie close to a body's surface, as it presents an asymptotic behavior when evaluating induced velocities in the vicinity of the vortex segment. Such behavior results in non-physical near-infinite velocity values for those points. The Vatistas model allows for a more physical prediction of the velocities in such regions by introducing a vortex core. When the point of evaluation is located inside that core, the induced velocity decreases to zero. This model is widely used in rotor applications, in which the wake usually stays close to the rotor (especially in the hover and descent flight phases) [12, 13].

IV. Results

The parameters studied here are the horizontal and vertical distances between the wings (respectively D_x and D_z), the angle of attack and the dihedral angle of each wing (respectively $AOA_{f/a}$ and $Dih_{f/a}$, where f indicates the front wings and a the aft wings). Free stream velocities between 5 m/s and 30 m/s were tested in the wind tunnel in order to determine the speed at which the aerodynamic load coefficients are stabilized despite the increasing Reynolds number.

The lift and drag results will be presented for each case. For easier comparison, these forces were non-dimensionalised using the total surface of the wings ($S_{wing} = c\,b$) so that

$$C_L = \frac{L_{\text{tot}}}{0.5\,\rho\,U^2\,4S_{wing}} \qquad C_D = \frac{D_{\text{tot}}}{0.5\,\rho\,U^2\,4S_{wing}} \tag{1}$$

A. Reynolds independence analysis

Before any other experiment, a Reynolds independence analysis was conducted on the total system. The wings were placed at the same height ($D_z = 0$) and the spacing between the front wing's trailing edge and aft wing's leading edge was set to $D_x = 0.6\,c$. Both dihedral angles were set to 0° and the angles of attack were set to 6°. Fig.5 presents the variation of the lift and drag area coefficients with free stream velocity. These coefficients are calculated using the ratio of the force over the dynamic pressure :

$$C_L S = \frac{L_{\text{tot}}}{0.5\,\rho\,U^2} \qquad C_D S = \frac{D_{\text{tot}}}{0.5\,\rho\,U^2} \tag{2}$$

It can be observed that the load coefficients become nearly constant with airspeed above 18 m/s. Therefore, all the wind tunnel measurements presented in this work were obtained at an airspeed of 20 m/s. This results in a Reynolds of approximately 85,000.

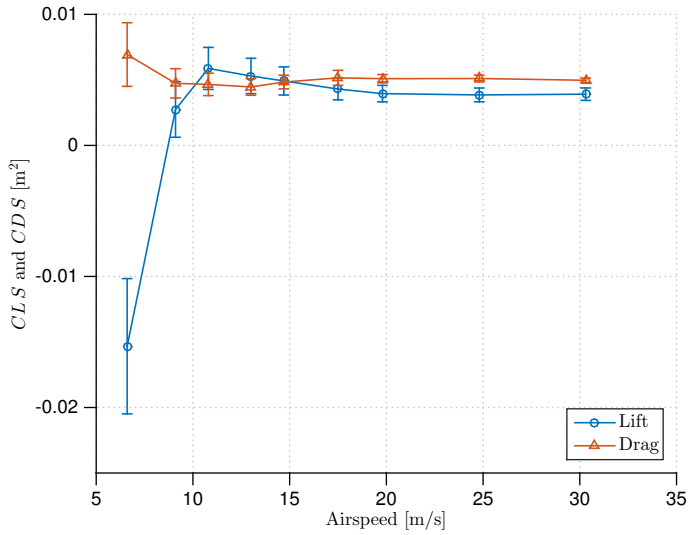

Fig. 5 $C_L S$ and $C_D S$ of the body and mount with respect to the free stream velocity.

B. Horizontal and vertical distance

The first parameter studied is the relative position of the two wings with respect to each other. The positions were defined using two parameters: D_x the separation along the x axis, measured from the front wing's trailing edge to the aft wing's leading edge; and D_z, the separation along the z axis, measured from the maximum thickness point of each wing (D_z is positive when the aft wing lies above the front wing). Throughout this section, the tests were carried out with no dihedral and with the angle of attack of the two sets of wings set to 6°. Fig. 6 presents the variation lift and drag coefficients with D_z for three different values of D_x.

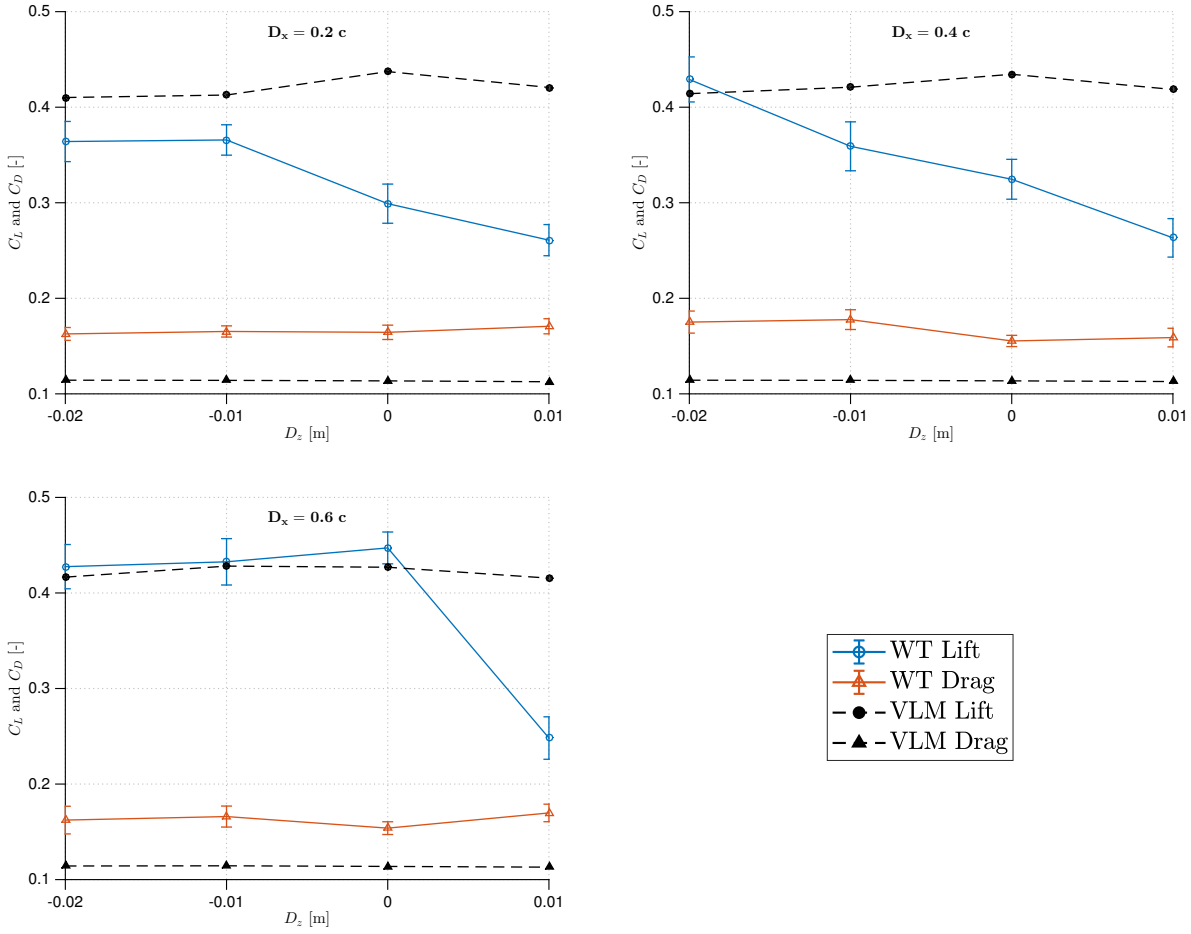

Fig. 6 Evolution of C_L and C_D of the total system with the vertical separation distance D_z, for three different horizontal separation D_x.

The first thing to notice is that the UVLM systematically underestimates the drag, which was expected as it is based on potential flow theory and therefore it does not model the viscous component of the total drag (only the viscous drag of the fuselage was added, the viscous drag of the wing could not be estimated from the experiments). In all cases, the drag is usually steady and is barely affected by the changes in D_z or D_x.

The lift on the other hand seems to be quite sensitive to the distance between the two wings. The wind tunnel measurements clearly show a significant decrease in lift when the aft wings are placed above the front wings. It is also clear that if the two sets of wings are close to each other in the x direction, the lift is more sensitive to a change in the z direction. This confirms the results presented in [14] for similar wing geometries at low Reynolds.

The UVLM predictions for the lift seem to be in agreement with the wind tunnel measurements only for large D_x and/or low D_z. Once again, these observations can be explained by the fact that the UVLM does not model viscous effects. When the aft wing is close to the front wing (small D_x), such effects may affect significantly the aerodynamics of the aft wing, especially when it lies inside the wake of the front wing. When the aft wings lie above the front wings, the high pressure under the latter may cause an additional adverse pressure gradient on the upper surface of the former, resulting in flow separation at lower angles of attack. These specific cases should be investigated further using flow visualization techniques or less restrictive numerical methods such as RANS solvers.

C. Angle of attack

This section focuses on the analysis of the effect of the angles of attack of the two wings. In this configuration, the two sets of wings are at the same height ($D_z = 0$) and separated horizontally by $D_x = 0.6c$. No dihedral is applied and only the wings' angles of attack are modified.

Fixed front wing

In this first case, the front wings' AOA is fixed to either 4° or 6° and the aft wings' angle of attack is changed. The results are presented in Fig. 7. For these two graphs, the UVLM matches very well the experimental measurements. Once again, the drag calculated with the numerical method is underestimated, due to the impossibility to account for the viscous drag of the wings.

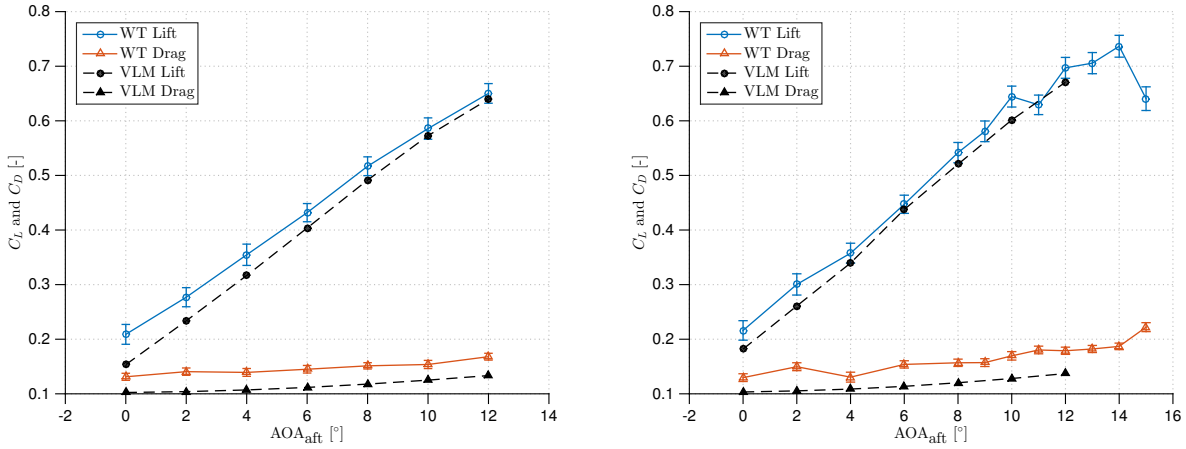

Fig. 7 Evolution of C_L and C_D of the total system with respect to the aft wing's angle of attack, for $AOA_{\text{front}} = 4°$ and $6°$ (resp. left and right).

In general, the lift increases linearly up to the stall angle. The wind tunnel tests were carried until stall is reached for the case where $AOA_{\text{front}} = 6°$. As the front wing induces some downwash on the aft wing, the effective angle of attack of the aft wing is decreased. This allows to push the stall of the entire system towards larger values of AOA_{aft}. Similar tests were conducted for other values of AOA_{front} ranging from 0° to 12° and all led to the same conclusions.

Fixed aft wing

In this case, the aft wings' AOA is fixed to either 4° or 6° and the front wings' angle of attack is changed. The results are presented in Fig. 8. These cases present a very interesting behavior. First of all, it is clear that the lift no longer increases linearly. The overall gradient is much lower than for the cases where the aft angle of attack was changed (as in Fig. 7). When the front wings are pitched to 8°, the system seems to stall according to the wind tunnel results (the UVLM can not model stall). When the front wings' angle of attack is increased further, the lift recovers initially but the system stalls once again between 10° and 12°. At this point the stall induces buffeting on both sets of wings. This phenomenon leads to strong vibrations, as indicated by the very large error bars. In general the VLM captures quite well the overall trend, despite its inviscid hypotheses, but it fails to predict the local lift decrease for $AOA_{\text{front}} = 8°$.

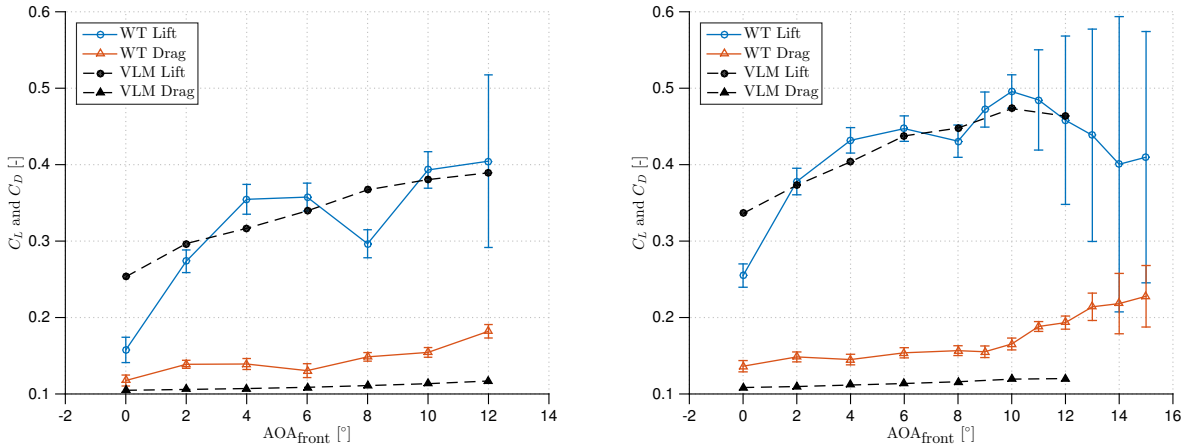

Fig. 8 Evolution of C_L and C_D of the total system with respect to the front wing's angle of attack, for $AOA_{\text{aft}} = 4°$ and 6° (resp. left and right).

It is not clear yet why a first stall seems to appear at $AOA_{\text{front}} = 8°$. The main hypothesis is that the front wing exhibits trailing edge stall at 8° because a high pressure zone builds up between the two wings. When the front wings' angle of attack is increased, the pressure may be reduced slightly thanks to a small increase in the available space between the two wings; this could lead to a reattachment of the flow. Finally when the angle of attack reaches approximately 11° the front wing completely stalls again, but this time from the leading edge. The flow behind the first set of wings is highly turbulent and causes severe buffeting. Further analysis with flow visualization techniques (such as Particle Image Velocimetry) should give more insight on the actual flow behavior at this attitude. It should also be mentioned that the drag is once again underestimated by the UVLM, especially when the flow is no longer attached.

The same tests were conducted for values of AOA_{aft} ranging from 0° to 12° and similar conclusions were drawn.

D. Dihedral

The last parameter to be studied is the dihedral angle. The two sets of wings were placed at the same height ($D_z = 0$) and separated horizontally by $D_x = 0.4c$. The front wing dihedral was varied between −6° and 12°, while the aft dihedral was varied between −24° and 12°. Note that negative values for the dihedral result in an anhedral configuration. Figure 9 plots the variation of the lift and drag coefficients with Dih_a for $Dih_f = -6°$, 0° and 12°.

In general, there is good agreement between the numerical predictions and the experimental measurements. However, the simulated lift seems to be slightly underestimated in comparison to the lift measured in the wind tunnel. As always, the UVLM drag is underestimated due to the lack of viscous modeling. Both the experimental and numerical data suggest that the drag is generally independent of the two dihedral angles.

The lift coefficient seems to be more sensitive to the aft dihedral than the front. The numerical solution tends to indicate that the lift is lower when the two sets of wings present exactly the same dihedral angle. The experimental data suggest that the lift decreases when the two dihedral angles are close to each other and that the lift is often better when the two sets of wings present a large difference in dihedral angle. It is quite notable that some configurations induce high lift without a significant increase in drag. This means that it is possible to maximize the lift and simultaneously maximize

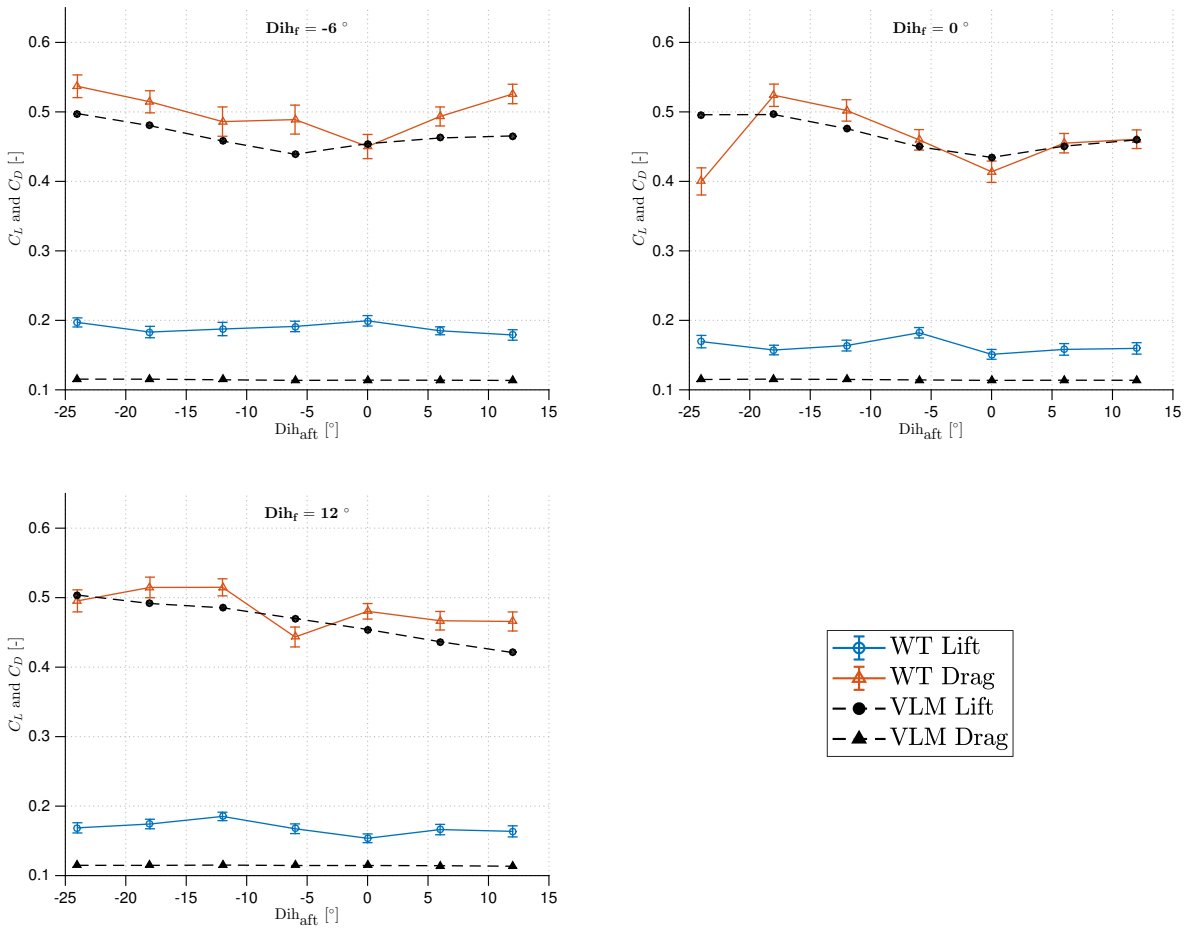

Fig. 9 Evolution of C_L and C_D of the total system with the aft dihedral angle, for three different values of the front dihedral.

the efficiency (defined as the lift-to-drag ratio) of the assembly. This result is important in the determination of the hind limb position of prehistorical flyers such as the *Microraptor* and seems to be in contradiction to the observations by [7].

V. Perspectives and conclusions

In most of the experiments the lift seems to be very well predicted by the numerical simulations, especially when the two wings do not lie too close to each other. However the drag is always underestimated by the UVLM, due to the method's inability to model interference and viscous drag. The large size of the fairing/fuselage with respect to the wings has also a considerable impact on the measurements, especially as the wing tip effects at the root are expected to be much lower in reality than in the numerical simulations.

Three major conclusions can already be drawn form this analysis. First, the distance between the two wings can lead to a significant change in the aerodynamic performance of the system. In the situation where the aft wings lie above the front ones, the lift can be reduced by 25% to 30%, without necessarily resulting in increased drag. When the two wings are close to each other (in the horizontal direction), the lift is also negatively impacted, mainly due to an increase in viscous drag.

The second important observation is that variations in the angle of attack result in different lift gradients if they are applied to the front or aft wings. When only the aft wings' angles of attack are increased, the forces increase linearly, as if the wings were isolated. The stall of the overall system is slightly delayed, thanks to the downwash induced from the front wings onto the aft wings. This downwash reduces the effective angle of attack seen by the aft wings, which in turn leads to delayed stall. Interestingly, it was shown that the variation of the angle of attack of the front wings leads to a nonlinear variation in the total lift. That lift curve slope is much lower than that of the aft wings, which means that the same change in the angle of attack of the front wings will result in a much lower lift increase than when the same change is applied to the aft wings. It was also shown that for the specific angle of attack value of 8° on the front wings, the complete system appears to stall. A further increase of this angle will lead to an increase of the system's lift until a second complete stall occurs with significant buffeting.

Finally, the third main observation is that the dihedral angle pays an important role in the lift generated by the system. It was shown that the system benefits from a larger lift when the aft and front wings have very different dihedral values. In all cases, the total lift was proven to be smaller when the two angles are similar. The drag coefficient was also proven to be insensitive to the dihedral angle variation. This leads to the conclusion that some specific combinations of dihedral angle lead to lift maximization, while also ensuring maximum efficiency (highest lift-to-drag ratio).

Some interesting phenomena are still not properly understood (especially the stall when the front wing is pitched at 8°). Flow visualization techniques such as Particle Image Velocimetry should shed light on the behavior of the flow around the wings and help determine the reason behind these observations. This entire analysis will also be extended to cambered airfoils (of NACA 6409 type). Subsequently, more realistic geometries (based on a goose wing) will be studied. Once the full impact of each parameter is quantified, the in-flight attitude of four-winged biological entities such as the *Microraptor* will be inferred.

References

[1] Miles, G. H., "The Tandem Monoplane Its Merits and Drawbacks Compared with those of Tailless, Tail first and Allwing Designs : Libellula Suggested as Name for Class," *Flight*, 27 April 1944.

[2] Warkentin, J., and DeLaurier, J., "Experimental Aerodynamic Study of Tandem Flapping Membrane Wings," *Journal of Aircraft*, Vol. 44, No. 5, 2007, pp. 1653–1661. doi:10.2514/1.28160.

[3] Michelson, R. C., "Novel approaches to miniature flight platforms," *Proceedings of the Institution of Mechanical Engineers, Part G: Journal of Aerospace Engineering*, Vol. 218, No. 6, 2004, pp. 363–373. doi:10.1243/0954410042794911.

[4] Xu, X., Zhou, Z., Wang, X., Kuang, X., Zhang, F., and Du, X., "Four-winged dinosaurs from China." *Nature*, Vol. 421, No. 6921, 2003, pp. 335–40. doi:10.1038/nature01342.

[5] Chatterjee, S., and Templin, R. J., "Biplane wing planform and flight performance of the feathered dinosaur Microraptor gui," *Proceedings of the National Academy of Sciences*, Vol. 104, No. 5, 2007, pp. 1576–1580. doi:10.1073/pnas.0609975104.

[6] Alexander, D. E., Gong, E., Martin, L. D., Burnham, D. A., and Falk, A. R., "Model tests of gliding with different hindwing configurations in the four-winged dromaeosaurid Microraptor gui," *Proceedings of the National Academy of Sciences*, Vol. 107, No. 7, 2010, pp. 2972–2976. doi:10.1073/pnas.0911852107.

[7] Dyke, G., De Kat, R., Palmer, C., Van Der Kindere, J., Naish, D., and Ganapathisubramani, B., "Aerodynamic performance of the feathered dinosaur Microraptor and the evolution of feathered flight," *Nature Communications*, Vol. 4, 2013, pp. 1–9. doi:10.1038/ncomms3489.

[8] Katz, J., and Plotkin, A., *Low-Speed Aerodynamics*, 2nd ed., Cambridge Univesity Press, New-York, USA, 2013. doi:10.1017/CBO9780511810329.

[9] Lambert, T., and Dimitriadis, G., "Induced Drag Calculations with the Unsteady Vortex Lattice Method for Cambered Wings," *AIAA Journal*, Vol. 55, No. 2, 2017, pp. 687–672.

[10] Lambert, T., Abdul Razak, N., and Dimitriadis, G., "Vortex Lattice simulations of attached and separated flows around flapping wings," *Aerospace*, Vol. 4, No. 2, 2017, p. 22.

[11] Vatistas, G. H., Kozel, V., and Mih, W. C., "A simpler model for concentrated vortices," *Experiments in Fluids*, Vol. 11, No. 1, 1991, pp. 73–76. doi:10.1007/BF00198434.

[12] Ananthan, S., and Leishman, J. G., "Role of Filament Strain in the Free Vortex Modeling of Rotor Wakes," *Journal of the American Helicopter Society*, Vol. 49, No. 2, 2004, pp. 176–191. doi:10.1051/proc:1996039.

[13] Leishman, J. G., "Challenges in Modeling the Unsteady Aerodynamics ofWind Turbines," *21st ASME Wind Energy Symposium and the 40th AIAA Aerospace Sciences Meeting,*, 2002.

[14] Jones, R., Cleaver, D. J., and Gursul, I., "Aerodynamics of biplane and tandem wings at low Reynolds numbers," *Experiments in Fluids*, Vol. 56, No. 6, 2015, p. 124. doi:10.1007/s00348-015-1998-3.

This is the final pre-print submitted to the AIAA.
The published version can be found on AIAA website.

doi:10.2514/6.2019-1620.